SAND2017-6264C

Dynamic Considerations of Power System Coupling through Dual-Wound Generators

L. J. Rashkin[1], J. C. Neely[1], S. F. Glover[1], T. J. McCoy[2], S. D. Pekarek[3]
[1]Sandia National Laboratories, Albuquerque, NM, USA
[2]McCoy Consulting, LLC, Box Elder, ND
[3]Dept. of Electrical and Computer Engineering, Purdue University, West Lafayette, IN
lrashki@sandia.gov

***Abstract*— Several technical power system architectures are being evaluated for the Navy's next generation all-electric warship. One concept being considered includes a scheme to power both port and starboard busses from a single generator with dual-windings. This approach offers redundancy and reduces the effects of prime mover light loading, but it inherently couples the two busses through the common generator. In this work, dynamic issues of galvanic and electro-mechanical coupling of power systems through a single dual-wound generator are discussed. Previous works focused on harmonics and galvanic coupling. Herein, focus is placed on average-value modeling of the galvanic coupling and on evaluation for fault response. Conclusions are presented from analysis, simulation, and experimental results.**

Keywords—dual wound machine, electric ship, average value modeling

I. Introduction

The primary purpose of a dual-wound machine is to supply multiple power systems from a single compact generator [1]. Several different winding strategies and applications can be applied to dual wound machines [1]-[3]. This can even include using two sets of windings with different frequencies to supply a high powered propulsion load as well as a lower powered service load [1], but should also allow for redundant systems where one generator can be used to supply power for both port and starboard busses [4]. Dual wound machines can also allow for a single machine to operate in both generation and motoring modes at the same time [2]. In some instantiations, this can allow for some simplification of power electronics and enables a connected battery to charge or discharge to one set of windings while the other set of windings is always used to provide power to electrical devices on the system [2]. Dual wound machines can also provide better power quality by tighter regulation of stator MMF [3]. In all the above cases, the machine windings are made to minimize flux linkages between the phases of different winding sets and their construction can be very different from traditional strategies.

The primary engineering challenge with dual wound machines is managing the galvanic and electromechanical coupling of the two circuits. Specifically, since the phase currents of both circuits contribute to flux linkage and torque, the loading of one circuit may couple to the other through the stator flux (galvanic) and/or through transient effects on mechanical speed (electro-mechanical). While the electro-mechanical coupling is somewhat intuitive and easily modeled, the galvanic coupling is more challenging. In this work, a 2-zone power system with dual-wound machine was modeled and evaluated in simulation for several fault scenarios. In particular, an average-value model was developed through extension of the approach laid out in [5]-[7], to capture the coupling between phases under different loading conditions. In addition, a scaled version of the system was evaluated in a laboratory-scale testbed.

The next section describes the 2-zone power system under evaluation and presents the models used for the key components. Section III provides simulation results for faulted and unfaulted scenarios. A scaled version of the system was evaluated in hardware on the Secure Scalable Microgrid Testbed (SSMTB) [8] and compared to simulation results; the system and results are described in Sections IV and V. Finally, conclusions and future work are described in Section VI.

II. Two-Zone Power System with Dual Wound Generator

In this work, a two-zone power system, wherein both zones are supplied by a single generator, is evaluated; see Fig. 1. The system includes a 10 kW rated gas-turbine generator with speed governor, a dual-wound permanent magnet synchronous machine (PMSM) , two passive rectifiers with LC output filters, switch gear, and variable resistive loads. Herein, two variations of the dual-wound machine are considered, including a symmetrical dual-wound PMSM (SDW-PMSM) and an asymmetrical dual-wound machine (ADW-PMSM).

It is noted that a larger scale system would likely include a synchronous machine with field winding and excitation system as well as active rectifiers; herein, the focus is on a system that is consistent with Sandia's SSMTB. The principal component models are described further in this section.

A. Gas Turbine Engine

The model for the gas turbine engine was derived from [9] and [10], which simplifies the system based on an empirical analysis of power flow. According to the derivation of [9], the model takes the form:

$$P_{fuel}^{*} = (c_6 + c_7\omega_{rm} + c_8\omega_{rm}^2 + c_9\omega_{rm}^3)u_{fuel} + (c_{10} + c_{11}\omega_{rm} + c_{12}\omega_{rm}^2 + c_{13}\omega_{rm}^3)(1 - u_{fuel}) \quad (1)$$

$$\frac{dP_{fuel}}{dt} = m_{rate}\tanh\left(\frac{P_{fuel}^{*} - P_{fuel}}{\tau_{fuel}m_{rate}}\right) \quad (2)$$

$$\frac{dP_{comp}}{dt} = k_5P_{comp} + k_6P_{fuel} \quad (3)$$

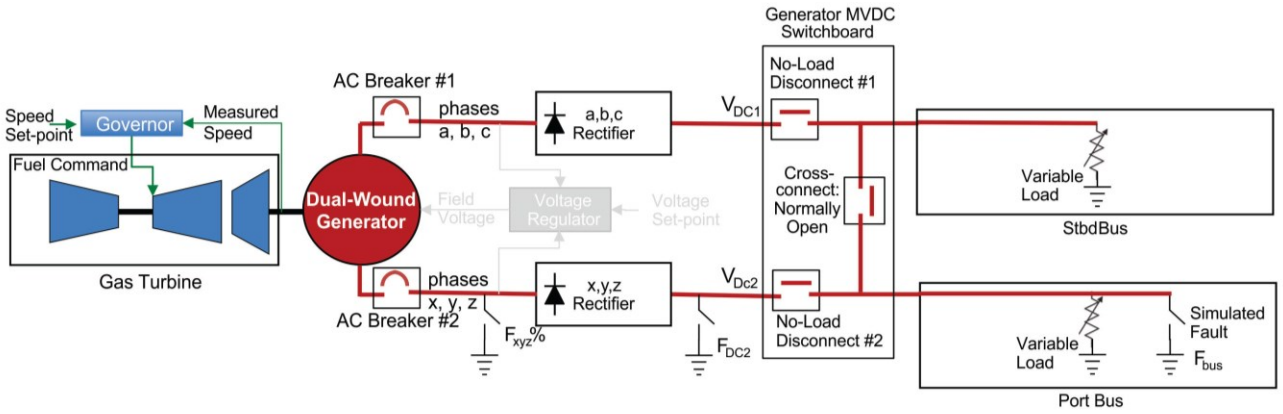

Figure 1: Illustration of Two Power Systems Supplied by a Single Generator

$$P_{wf3} = \eta_{comb} P_{fuel} + P_{comp} \quad (4)$$

$$P_{turb} = \left(c_1 + k_1 P_{wf3} + k_2 P_{wf3}^2\right)\omega_{rm} + \left(k_3 P_{wf3} + k_4 P_{wf3}^2\right)\omega_{rm}^2 \quad (5)$$

where P_{fuel}^* and P_{fuel} are the commanded and actual fuel power, P_{comp} and P_{wf3} are the power at the compressor and output shaft, u_{fuel} is the normalized control input between 0 and 1, m_{rate} is the maximum rate of change of fuel power, τ_{fuel} is the time constant of the fuel rate, and η_x is the efficiency of x.

The parameters c_1 through c_5 are based on a surface mapping of the relationship between steady state output power, steady state fuel power, and steady state speed. Parameters k_1 through k_5 are based on c_2 through c_5, τ_{comp}, and the efficiencies of the compressor, combustor, turbine, and extraction. The parameters c_6 through c_{13} determine polynomial fits to the minimum and maximum fuel power as functions of speed.

The output torque of the turbine, T_{turb}, can be determined by dividing the turbine output power by the shaft speed:

$$T_{turb} = \frac{P_{turb}}{w_{rm}} \quad (6)$$

The turbine speed is controlled through the use of a standard proportional + integral (PI) feedback control based governor. The control adjusts the mass flow rate of fuel in response to turbine speed error.

$$u_{fuel}(t) = K_P\left(\omega_{rm}^* - \omega_{rm}(t)\right) + K_I \int \left(\omega_{rm}^* - \omega_{rm}(t)\right) dt \quad (7)$$

where K_P and K_I are the proportional and integral coefficients respectively and are provided in Table 1.

B. *Dual wound generator*

For a round rotor permanent magnet machine with 6 phases, a reference frame transform can be constructed by considering the two 3-phase sets separately, with one referenced to the rotor position θ_r and one offset by an angle β as follows:

$$K_{s_{abc}}^r = \frac{2}{3}\begin{bmatrix} \cos(\theta_r) & \cos\left(\theta_r - \frac{2\pi}{3}\right) & \cos\left(\theta_r + \frac{2\pi}{3}\right) \\ \sin(\theta_r) & \sin\left(\theta_r - \frac{2\pi}{3}\right) & \sin\left(\theta_r + \frac{2\pi}{3}\right) \\ 1/2 & 1/2 & 1/2 \end{bmatrix} \quad (7)$$

$$K_{s_{xyz}}^r = \frac{2}{3}\begin{bmatrix} \cos(\theta_r - \beta) & \cos\left(\theta_r - \beta - \frac{2\pi}{3}\right) & \cos\left(\theta_r - \beta + \frac{2\pi}{3}\right) \\ \sin(\theta_r - \beta) & \sin\left(\theta_r - \beta - \frac{2\pi}{3}\right) & \sin\left(\theta_r - \beta + \frac{2\pi}{3}\right) \\ 1/2 & 1/2 & 1/2 \end{bmatrix} \quad (8)$$

$$K_s^r = \begin{bmatrix} K_{s_{abc}}^r & 0 \\ 0 & K_{s_{xyz}}^r \end{bmatrix} \quad (9)$$

where β denotes the pitch angle between the *abc* and *xyz* set of windings. The generator model is adjustable to run with offsets of 60^o or 30^o between the *abc*- and *xyz*-phases of the generator, termed *symmetrical* and *asymmetrical* respectively. The machine equations in this reference frame can be written as:

$$v_{qs_{abc}}^r = r_s i_{qs_{abc}}^r + \omega_r \lambda_{ds_{abc}}^r + p\lambda_{qs_{abc}}^r \quad (10)$$

$$v_{qs_{xyz}}^r = r_s i_{qs_{xyz}}^r + \omega_r \lambda_{ds_{xyz}}^r + p\lambda_{qs_{xyz}}^r \quad (11)$$

$$v_{ds_{abc}}^r = r_s i_{ds_{abc}}^r - \omega_r \lambda_{qs_{abc}}^r + p\lambda_{ds_{abc}}^r \quad (12)$$

$$v_{ds_{xyz}}^r = r_s i_{ds_{xyz}}^r - \omega_r \lambda_{qs_{xyz}}^r + p\lambda_{ds_{xyz}}^r \quad (13)$$

$$v_{0s_{abc}}^s = r_s i_{0s_{abc}}^r + p\lambda_{0s_{abc}}^r \quad (14)$$

$$v_{0s_{xyz}}^s = r_s i_{0s_{xyz}}^r + p\lambda_{0s_{xyz}}^r \quad (15)$$

$$\lambda_{qs_{abc}}^r = \left(L_{ls} + \frac{3}{2}L_{ms}\right) i_{qs_{abc}}^r + \frac{3}{2}L_{ms} i_{qs_{xyz}}^r \quad (16)$$

$$\lambda_{qs_{xyz}}^r = \left(L_{ls} + \frac{3}{2}L_{ms}\right) i_{qs_{xyz}}^r + \frac{3}{2}L_{ms} i_{qs_{abc}}^r \quad (17)$$

$$\lambda_{ds_{abc}}^r = \left(L_{ls} + \frac{3}{2}L_{ms}\right) i_{ds_{abc}}^r + \frac{3}{2}L_{ms} i_{ds_{xyz}}^r + \lambda'_m \quad (18)$$

$$\lambda_{ds_{xyz}}^r = \left(L_{ls} + \frac{3}{2}L_{ms}\right) i_{ds_{xyz}}^r + \frac{3}{2}L_{ms} i_{ds_{abc}}^r + \lambda'_m \quad (19)$$

$$\lambda_{0s_{abc}}^r = L_{ls} i_{0s_{abc}}^r \quad (20)$$

$$\lambda_{0s_{xyz}}^r = L_{ls} i_{0s_{xyz}}^r \quad (21)$$

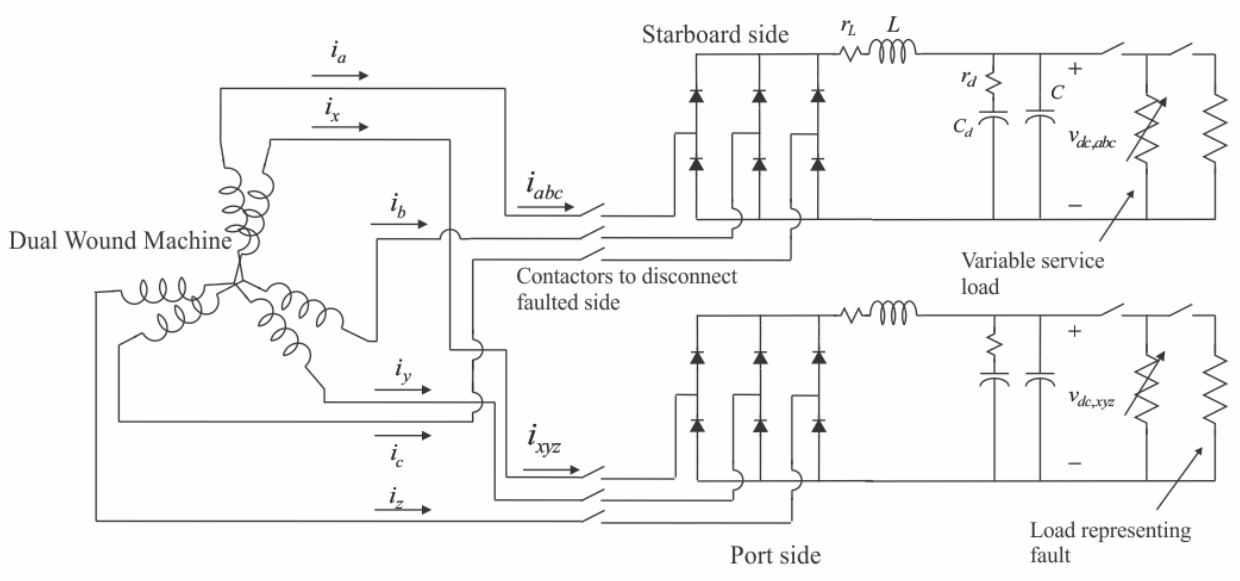

Figure 2: Electrical schematic of generator, rectifier, LC filter, and loads

where $f_{qs_{abc}}$, $f_{ds_{abc}}$, and $f_{0s_{abc}}$ denote the variable f from the *abc* set of phases in the *qd0*-axis and $f_{qs_{xyz}}$, $f_{ds_{xyz}}$, and $f_{0s_{xyz}}$ denote the variable f from the *xyz* set of phases in the *qd0*-axis.

The electromagnetic torque may be expressed in the *qd*-axis as [11],[12]:

$$T_{elec} = \frac{3}{2}\frac{P}{2}\lambda'_m\left(i^r_{qs_{abc}} + i^r_{qs_{xyz}}\right) \tag{22}$$

wherein P is the number of poles, $i^r_{qs_{abc}}$ is q-axis current associated with the *abc* set of phases, $i^r_{qs_{xyz}}$ is the q-axis current associated with the *xyz* set of phases, and λ'_m is the flux linkage contributed by the permanent magnet.

C. Average-value rectifier model

Since the system involves both an electrical response and a mechanical response, it is helpful to develop an average-value model (AVM) for the rectifier in order to reduce computational load. The AVM used is based on [6]-[8] which takes a detailed switch level model of the rectifier and processes the response to a continuously changing load. The results of this detailed simulation are then used to determine relationships between the DC variables and AC variables. Herein, the method is adapted to include two electrical 3-phase windings and two rectifiers.

In general, the model for a single rectifier can be parameterized for the fast average values around a dynamic impedance relating the output voltage, $\bar{v}_c$, to the magnitude of the input currents, $\|\bar{\imath}_{qds}\|$

$$z = \frac{\bar{v}_c}{\|\bar{\imath}_{qds}\|} \tag{23}$$

Algebraic estimations can be formulated for the remaining variables based on parameterization around the dynamic impedance:

$$\delta_r = \arctan\left(\frac{i^r_{ds}}{i^r_{qs}}\right) - \phi(z) \tag{24}$$

$$\bar{v}^r_{qs} = \alpha(z)\bar{v}_{dc}\cos(\delta_r) \tag{25}$$

$$\bar{v}^r_{ds} = \alpha(z)\bar{v}_{dc}\sin(\delta_r) \tag{26}$$

$$\bar{\imath}_{dc} = \beta(z)\|\bar{\imath}_{qds}\| \tag{27}$$

where $\alpha(z)$, $\beta(z)$, and $\phi(z)$ are look-up tables based on the results from the detailed simulation.

In a system with two rectifiers connected through a single dual wound synchronous generator, the behavior of one rectifier will have a dynamic effect on the performance of the other. Therefore, the parameterizations need to take the dynamic impedance of both rectifiers into account. Herein, this is accomplished using expressions:

$$z_{abc} = \frac{\bar{v}_{c_{abc}}}{\|\bar{\imath}_{qds_{abc}}\|} \tag{28}$$

$$z_{xyz} = \frac{\bar{v}_{c_{xyz}}}{\|\bar{\imath}_{qds_{xyz}}\|} \tag{29}$$

$$\delta_{r_{abc}} = \arctan\left(\frac{\bar{\imath}^r_{ds_{abc}}}{\bar{\imath}^r_{qs_{abc}}}\right) - \phi_{abc}(z_{abc}, z_{xyz}) \tag{30}$$

$$\bar{v}^r_{qs_{abc}} = \alpha_{abc}(z_{abc}, z_{xyz})\bar{v}_{dc_{abc}}\cos(\delta_{r_{abc}}) \tag{31}$$

$$\bar{v}^r_{ds_{abc}} = \alpha_{abc}(z_{abc}, z_{xyz})\bar{v}_{dc_{abc}}\sin(\delta_{r_{abc}}) \tag{32}$$

$$\bar{\imath}_{dc_{abc}} = \beta_{abc}(z_{abc}, z_{xyz})\|\bar{\imath}_{qds_{abc}}\| \tag{33}$$

$$\delta_{r_{xyz}} = \arctan\left(\frac{\bar{\imath}^r_{ds_{xyz}}}{\bar{\imath}^r_{qs_{xyz}}}\right) - \phi_{xyz}(z_{abc}, z_{xyz}) \tag{30}$$

$$\bar{v}^r_{qs_{xyz}} = \alpha_{xyz}(z_{abc}, z_{xyz})\bar{v}_{dc_{xyz}}\cos\left(\delta_{r_{xyz}}\right) \tag{31}$$

$$\bar{v}^r_{ds_{xyz}} = \alpha_{xyz}(z_{abc}, z_{xyz})\bar{v}_{dc_{xyz}}\sin\left(\delta_{r_{xyz}}\right) \tag{32}$$

$$\bar{\imath}_{dc_{xyz}} = \beta_{abc}(z_{abc}, z_{xyz})\left\|\bar{\imath}_{qds_{xyz}}\right\| \tag{33}$$

These equations are different from those used in [8] due to the necessity of supplying two independent loads requiring separate q- and d-currents for each phase set.

III. Simulation Model

To evaluate the dynamics, simulation models were generated in Matlab that include the dual wound generator as

well as the gas turbine prime mover, a passive diode rectifier with LC output filter, and step-wise resistive load. The gas turbine generator was incorporated into the simulation using the empirically derived model found in [9]. The machine model was implemented using a Matlab ordinary differential equation (ODE) solver for equations 10-22. The rectifier was modeled both as a detailed switch model and using the AVM method described in Section II. A more detailed schematic is shown in Fig. 2, and Table 1 provides values used in the model. For the sake of brevity, the GTG parameters c_1-c_{13} and k_1-k_6 are omitted here, but were scaled from values available in [9].

Table 1: System parameters

Parameter	Symbol	Value	Units
Governor Integral Coeff.	K_I	0.0195	Watt/rad
Governor Proportional Coeff.	K_P	0.0234	Watt x sec/rad
GTG rotor inertia	J	0.63264	kg x m^2
Machine phase resistance	r_s	0.276	Ω
Machine magnetizing inductance	L_{ms}	3.50E-02	mH
Machine leakage inductance	L_{ls}	0.02	mH
Permanent Magnet Flux Linkage	λ_m	0.0703	volt-sec
Rectifier LC filter inductance	L	8	mH
Rectifier LC filter inductor ESR	r_L	0.22	Ω
Rectifier LC filter capacitance	C	1	mF
Rectifier LC filter damping capacitance	C_d	7	mF
Rectifier LC damping resistance	r_d	0.86	Ω

Calibration of the AVM model required several simulations be done first using the detailed model. Fig. 3 shows a comparison between the responses of the detailed model and the average-value model to a step change in load on the *abc*-side of the generator. The AVM remains a close match even on the unchanged side of the generator.

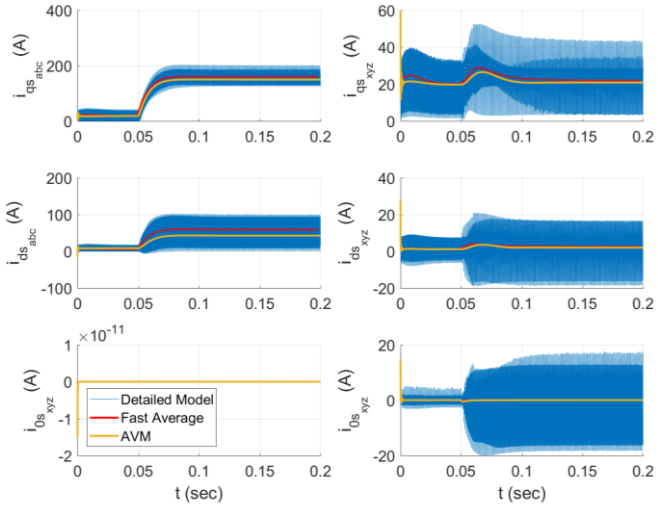

Figure 3 Comparison between detailed model and AVM for a low impedance fault of 1 Ω at 0.05 seconds

IV. Simulation Results

The AVM system models for both SDW-PMSM and ADW-PMSM configurations were simulated for a fault scenario representing a DC fault followed by an opening of an AC breaker. The simulation was run for 5 seconds with a short circuit fault occurring on the DC side of the *xyz* phase set at t = 0.05 seconds. The AC side of the *xyz* phase set was then open circuited at t = 0.15 seconds to clear the fault. These results are shown in Fig. 4. From the results it can be seen that over short timescales the galvanic coupling between windings does result in a response on the unfaulted winding set when a fault is placed on the other winding set.

Over longer time scales, the electromechanical coupling becomes a more important factor. Even after the breaker has opened, it takes some time for the speed governor to correct for the lost speed. The results show that there is very little difference in the performance of the 30° and 60° systems on the DC side. The DC voltage is 137 V at steady state when the fault occurs, but drops to 117 V during the fault and overshoots to 150 V after the breaker opens. This represents a 14.6% maximum deviation from the steady state value on the unfaulted side of the machine. This is a very large deviation and could exceed tolerances of the system. This problem could be solved with faster fault sensing and a faster breaker system.

V. Laboratory Scale Electric Ship Representation

The dynamic response was evaluated in hardware using the Secure Scalable Microgrid Test Bed (SSMTB). This section provides an overview of the testbed components used for the dual-wound generator experiment and presents the hardware results.

A. Microgrid Testbed Description

The SSMTB was developed to validate controls for networked microgrids [8] and was later configured to represent an all-electric ship power system with multiple busses (or zones) [13],[14]. The testbed includes three microgrid systems, a central bus cabinet for connecting components and microgrids, control computers, a data acquisition system, and a graphical user interface. The testbed is designed to operate at voltages up to 400 V dc; primary components include: several PMSM generators (6.5-10.0 kW), several 5 kW rated energy storage emulators, commercial motor drives with custom controls to emulate different rotational generators, and high-power digital resistors (0-6.7 kW), among other components. In addition, a master control console scripts the experiments with designated source and load profiles to ensure that experiments with highly variable sources and loads are run exactly the same each time. The laboratory layout is pictured in Fig. 5, along with some key components used in this work; these include the passive rectifier and digital resistor.

In addition, for this work, the SSMTB's electromechanical emulator [15]-[17] was modified to mimic the dynamics of a GTG with governor. The GTG model matches closely the one developed in [9], but scaled down as described in Section III. A custom 10 kW rated Georator [18] generator was developed, installed, and configured to act as a SDW-PMSM; see Fig. 6. The next subsection describes an experiment to validate the simulation model described in Sections II and III.

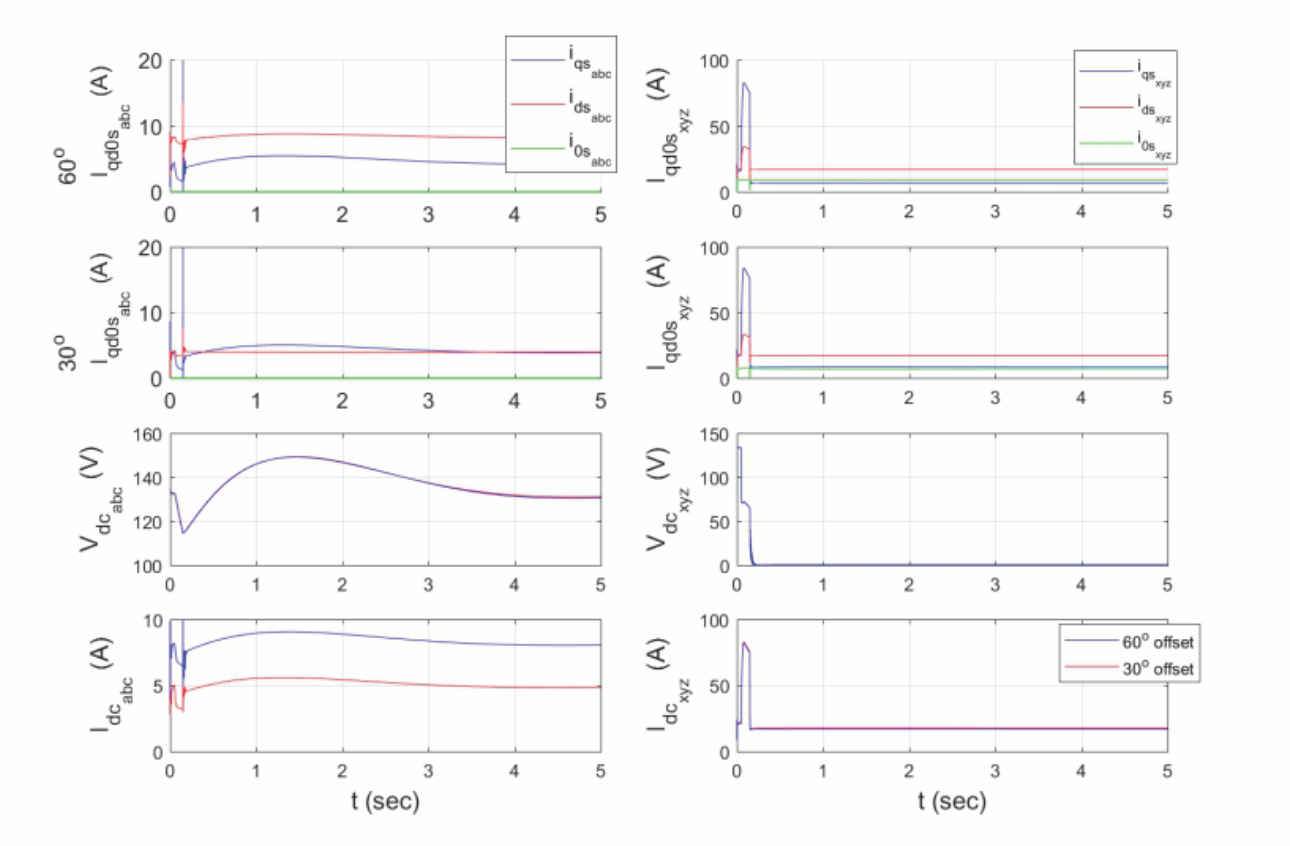

Figure 4: Fault response for unfaulted (left) and faulted (right) sides of machines with a 60° and 30° offset

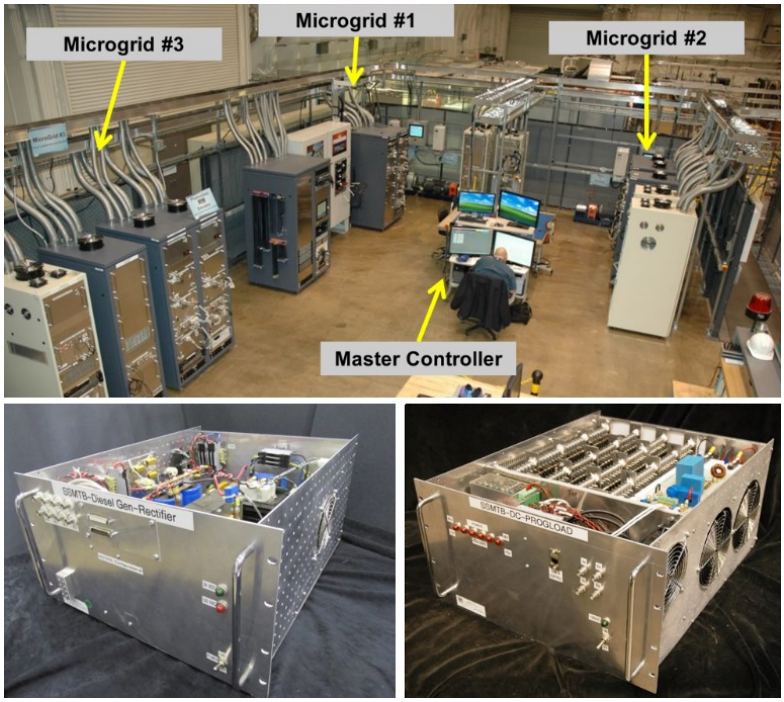

Figure 5: Photos of (top) the microgrid testbed including three interconnectable microgrids and select components including (bottom left) passive rectifier with LC output filter, and (bottom right) 6.7 kW digital resistor.

Figure 6: The mechanical source emulator is shown with ABB ACS800 drive, custom programmable feedback controller, Baldor 15 HP induction motor, and 10 kW SDW-PMSM installed with two 3-phase windings. The emulator was programmed to emulate the dynamics of a gas-turbine generator.

B. Variable Loading Experiment

An experiment was run with the generator commanded to a speed of 850 rpm and the resistive loads on each bus were varied in both steps and ramps between 50 Ω and 27.8 Ω over a 120 second profile. The load profiles are shown below in Fig. 7. The load profile is displayed this way since it gives a more intuitive depiction of loading since it is approximately proportional to load current.

A screenshot of the master control graphical interface following an experiment with the above load profile is shown in Fig. 8.

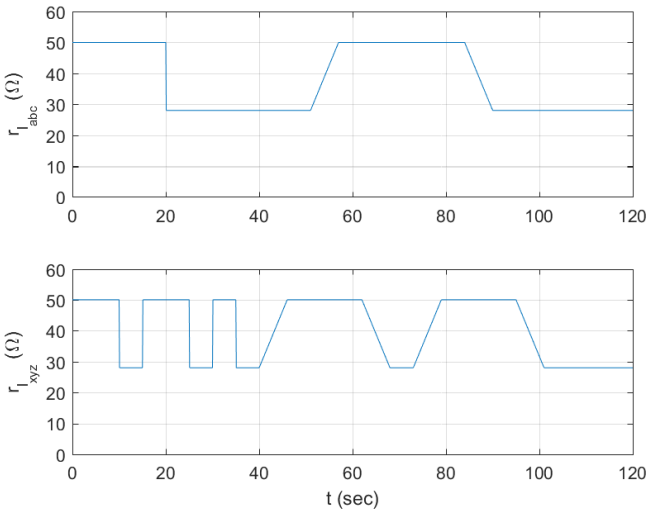

Figure 7: Load profile for (top) Starboard bus and (bottom) port side bus.

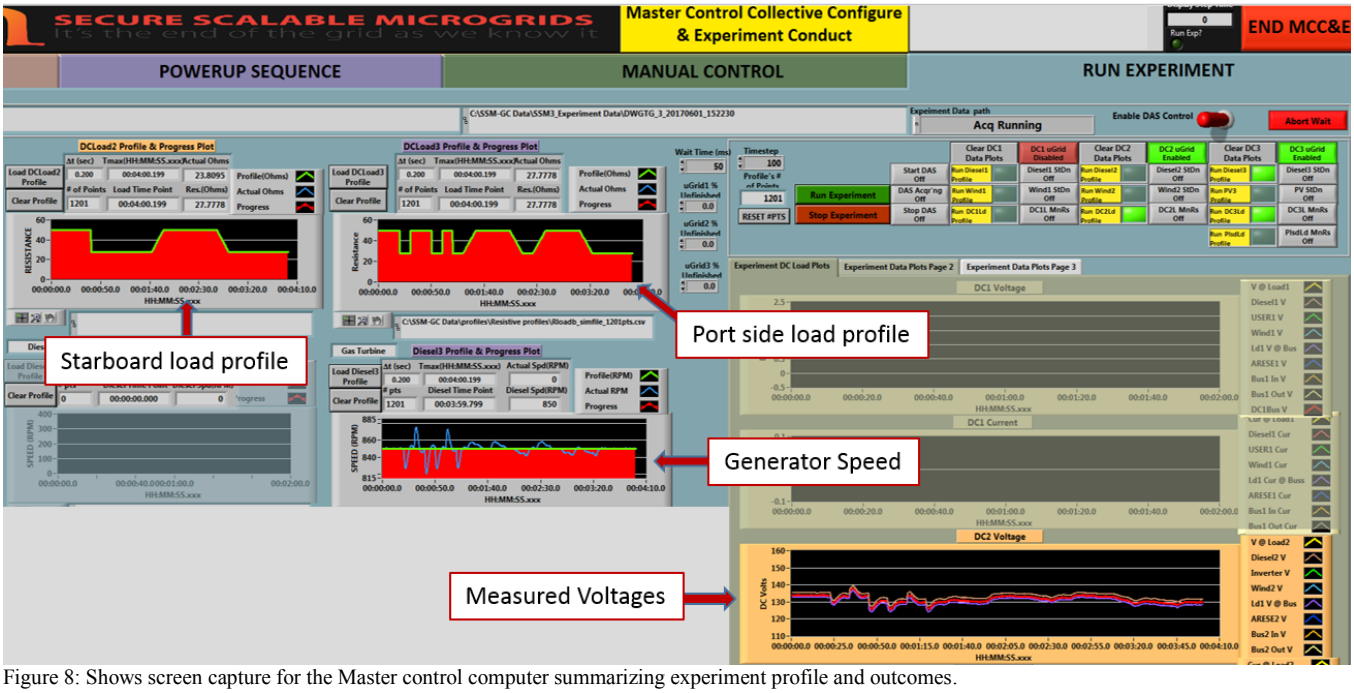

Figure 8: Shows screen capture for the Master control computer summarizing experiment profile and outcomes.

The experimental results and simulated results are compared in Fig. 9. The graph shows the measured data, a fast average of the measured data, and the results from a simulation of the system using the same operating conditions and load profile. The model correlates to the measured data well with little error. The simulated speed response is shown in Fig. 10. The simulated speed response matches the experimental response shown in Fig. 8. Table 2 quantifies the simulation and experimental results given the same scenario. Therein, the RMS error and Spearman correlation coefficient are also computed for the simulated and hardware results of each bus. The simulated data shows a high degree of correlation with the measured data as shown by Spearman coefficients close to 1. Additionally, RMS error is less than 1.05% of the mean.

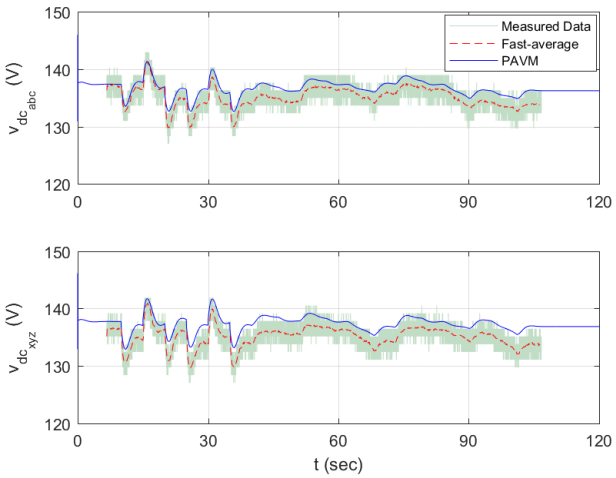

Figure 9: DC output voltage response to load profile

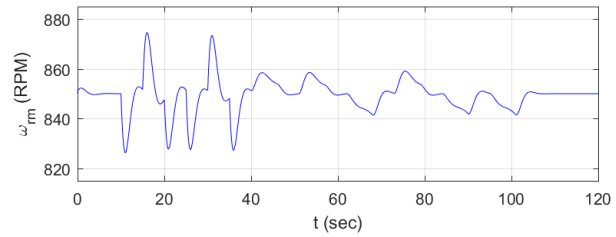

Figure 10: Generator speed response to load profile

Table 2: Comparison of Simulation and Hardware results (*abc* bus quantities appear above *xyz* bus quantities)

Metric	Simulation	Hardware	Units
Max bus voltages	140.72	141.22	Volts
	141.08	140.92	
Min bus voltages	131.59	129.78	Volts
	131.87	129.70	
Mean bus voltages	135.83	135.13	Volts
	136.56	135.12	
Max deviations	3.60	4.50	%
	-3.43	4.30	
Spearman Coefficient	0.9425		-
	0.8809		
RMS errors	0.9609		Volts
	1.4295		

VI. Summary and Future Work

In this paper, an analysis of the dynamics of a power system with dual-wound generator was performed. Both a detailed and an average-value model of a laboratory-scale system was developed; this model included an empirical gas turbine model, detailed models of a six-phase synchronous machine, and an average value modelled rectifier that was developed through parameterization of a detailed simulation of the system. The system was replicated in hardware and used to validate the results of the model. The model was then used to analyze the system response under fault conditions.

Future work will focus on modeling and simulating larger MW-scale power systems supplied by a dual wound machine. Model enhancements will be made to more closely replicate a practical shipboard system, including the addition of an excitation system and active rectifiers to the generator as well as the use of more representative load models. In addition, hardware experiments using an asymmetrical dual-wound machine configuration will be done to validate asymmetrical machine models and to further explore differences in performance between the different machine configurations.

Acknowledgment

This work was supported by NAVSEA for a project entitled *Nonlinear Power Flow Control Design for NGIP Energy Storage Requirements*, PR# 1400354102. The authors wish to thank, in particular, Norbert Doerry for discussion of dual wound machine implementation.

The authors also wish to thank Forest White, Todd Hendrickson, Mike Horry, and John Brown for their contributions to the hardware testbed and Dave Wilson for his guidance and leadership on this project.

Sandia National Laboratories is a multi-mission laboratory managed and operated by National Technology and Engineering Solutions of Sandia, LLC., a wholly owned subsidiary of Honeywell International, Inc., for the U.S. Department of Energy's National Nuclear Security Administration under contract DE-NA0003525.

This paper was approved under SAND number XXXX

References

[1] C. G. Hodge and J. F. Eastham, "Dual wound machines for electric ship power systems," *2015 IEEE Electric Ship Technologies Symposium (ESTS)*, pp. 62-67, Jun., 2015.

[2] E. Mese *et al.*, "A permanent magnet synchronous machine with motor and generator functionalities in a single stator core," *Compumag 2013,* Jul., 2013.

[3] E. Mese *et al.*, "Design considerations for dual winding permanent magnet synchronous machines," *2012 IEEE Energy Conversion Congr. and Expo. (ECCE)*, pp. 1894-1901, Sept., 2012.

[4] N. Doerry and J. Amy Jr., "The Road to MVDC," presented at ASNE Intelligent Ships Symposium 2015, Philadelphia, PA, May 20-21, 2015.

[5] J. Jatskevich, S. D. Pekarek, and A. Davoudi, "Parametric Average-Value Model of Synchronous Machine-Rectifier Systems," *IEEE Trans. Energy Convers.*, vol. 21, no. 1, pp. 9-18, Mar., 2006.

[6] J. Jatskevich, S. D. Pekarek, and A. Davoudi, "Fast Procedure for Constructing an Accurate Dynamic Average-Value Model of Synchronous Machine-Rectifier Systems," *IEEE Trans. Energy Convers.*, vol. 21, no. 2, pp. 435-441, Jun., 2006.

[7] J. Jatskevich and S. D. Pekarek, "Six-phase synchronous generator-rectifier parametric average value modeling considering operational models," *HAIT Journal of Science and Engineering B,* vol. 2, no. 3-4, pp. 365-385, 2005.

[8] S. F. Glover *et al.*, "Secure Scalable Microgrid Test Bed at Sandia National Laboratories," *IEEE Cyber-2012 Conference*, Bangkok, Thailand, May 27-31, 2012.

[9] C. J. Doktorcik, "Modeling and Simulation of a Hybrid Ship Power System" M.S. thesis, Dept. Elect. Eng., Purdue Univ., IN, 2011.

[10] R. T. Meyer, R. A. DeCarlo, S. Pekarek, and C. J. Doktorcik, "Gas Turbine Engine Behavioral Modeling," School of Elect. Eng., Purdue Univ., West Lafayette, Tech. Rep. TR-ECE-14-01, 2014.

[11] M. R. Aghaebramhimi and R. W. Menzies, "A Transient Model for the Dual Wound Synchronous Machine," *Canadian Conference on Elect. and Comput. Eng. 1997*, vol. 2, pp. 862-865, 1997.

[12] P. C. Krause, O. Wasynczuk, and S. D. Sudhoff, *Analysis of Electric Machinery and Drive Systems*, 2nd ed. Hoboken: John Wiley & Sons, Inc.

[13] D. Wilson *et al.*, "Hamiltonian Control Design for DC Microgrids with Stochastic Sources and Loads with Applications," *International Symposium on Power Electronics, Electrical Drives, Automation and Motion (SPEEDAM)*, Ischia, Italy, Jun. 18-20, 2014.

[14] J. C. Neely *et al.*, "Evaluation of Power Flow Control for an All-Electric Warship Power System with Pulsed Load Applications," *Applied Power Electronics Conference and Exposition (APEC) 2016,* Long Beach, CA, March 20-24, 2016.

[15] J. C. Neely *et al.*, "An economical diesel engine emulator for micro-grid research," *International Symposium on Power Electronics, Electrical Drives, Automation and Motion (SPEEDAM)*, Sorrento, Italy, Jun. 20-22, 2012,.

[16] J. C. Neely, S. F. Glover, O. Wasynczuk, and B. Loop, "Wind turbine emulation for intelligent microgrid development," *IEEE Cyber-2012 Conference*, Bangkok, Thailand, May 27-31, 2012.

[17] J. C. Neely *et al.*, "Electromechanical Emulation of Hydrokinetic Generators for Renewable Energy Research," *IEEE OCEANS 2013 Conference*, San Diego, CA, Sept. 23-26, 2013.

[18] URL: http://www.georator.com/